

## Three-dimensional atomic force microscopy based on tailored cantilever probe with flared tip

ZHANG Rui<sup>1,2</sup>, WU Sen<sup>1,2</sup>, XIAO Sha-sha<sup>1,2</sup>, HU Xiao-dong<sup>1,2</sup>, SHI Yu-shu<sup>3</sup>, FU Xing<sup>1,2</sup>

(1. State Key Laboratory of Precision Measurement Technology and Instruments, Tianjin University, Tianjin 300072, China;

2. Nanchang Institute for Microtechnology of Tianjin University, Tianjin 300072, China;

3. National Institute of Metrology, Beijing 100029, China)

**Abstract:** In order to meet the requirements of nondestructive testing of true 3D topography of micro-nano structures, a novel three-dimensional atomic force microscope (3D-AFM) based on flared tip is developed. A high-precision scanning platform is designed to achieve fast servo through moving probe and sample simultaneously, and several combined nanopositioning stages are used to guarantee linearity and orthogonality of displacement. To eliminate the signal deviation caused by AFM-head movement, a traceable optical lever system is designed for cantilever deformation detection. In addition, a method of tailoring the cantilever of commercial probe with flared tip is proposed to reduce the lateral force applied on the tip in measurement. The tailored probe is mounted on the 3D-AFM, and 3D imaging experiments are conducted on different samples by use of adaptive-angle scanning strategy. The results show the root-mean-square value of the vertical displacement noise (RMS) of the prototype is less than 0.1 nm and the high/width measurement repeatability (peak-to-peak) is less than 2.5 nm.

**Key words:** three-dimensional atomic force microscope (3D-AFM); flared tip; scanner; optical lever; vector scanning

**CLD number:** TH711

**doi:** 10.3969/j.issn.1674-8042.2020.04.011

### 0 Introduction

Recently, three-dimensional atomic force microscope (3D-AFM) has attracted more and more attention in the field of high-end industrial manufacturing because it allows nondestructive measurement of true 3D topography at nanoscale. For example, with the advancement of semiconductor technology, the size of field effect transistor (FET) continues to shrink. Meanwhile, the architecture of FET shifts from planar to 3D to make the gate voltage effectively turn off the conductive channel. Because the gate topography can affect the electrical performance of FET, 3D imaging is required to monitor the manufacturing process. Besides, sensors and actuators on MEMS chips have more complex 3D structure than FETs, which further makes a challenge to measurement technology.

Traditional AFM can only obtain 2.5D images due to the convolution effect of conical tip, while 3D-AFM achieves true 3D measurement by improving instrument structures and control methods<sup>[1-3]</sup>. Considering the working principles, 3D-AFM in

general can be divided into two types: the technology based on tilt scanning<sup>[4-5]</sup> and the technology base on flared tip<sup>[6-7]</sup>. The former is to rotate probe or sample so that the bottom of tip is able to touch horizontal surfaces and steep sidewalls. However, the probe for tilt scanning should be specially designed to avoid possible interference. Hence, Murayama et al designed a tilted tip on the probe instead of rotating probe<sup>[8]</sup>. Cho et al designed a cantilever with a width of less than 500 nm on 6  $\mu\text{m}$  wide wedge-shaped base. Therefore, the probe can work at tilt degree more than 40°<sup>[9]</sup>. They also developed a complicated rotatable AFM-head to ensure that the optical path for detecting cantilever deformation is not disturbed by tilting, whereas the tilted tip can only measure sidewalls in one direction. The tilt angle needs to be changed for obtaining the opposite sidewall images. This process will inevitably introduce rotation error in results. To solve this problem, Xie et al reported a dual-probe architecture in which two cylindrical fiber probes are mounted on AFM-head<sup>[10-11]</sup>. Before measuring, the relative position of two tips that are tilted in opposite directions is calibrated by scanning

**Received date:** 2020-07-08

**Foundation items:** National Key Research and Development Program of China (No. 2016YFF0200602); National Natural Science Foundation of China (No. 61973233)

**Corresponding author:** WU Sen (senwu@tju.edu.cn)

one tip with the other tip, and then sidewalls in different directions can be measured respectively. However, the tilt angle and the measuring depth are always limited by the aspect ratio of grooves.

In addition, a kind of probe with overhang characteristic on tip, which is called flared tip, is used for 3D measurement. This tip can reach steep sidewalls without tilting. In order to make flared tip be able to scan different surfaces, Martin et al proposed a tracking method coupled with a novel servo and scanning system<sup>[12]</sup>. The system can detect slope angle in real time and then adjust feedback direction and scanning direction. In this method, however, both scanning speed and slope gradient probably affect imaging results. Dai et al designed a special caliper which can excite probe to vibrate in vertical and torsional oscillation modes<sup>[13-14]</sup>. Surface profiling is achieved through vector approach probing strategy and the approaching angle of probe is programmed according to the profile from previous line scan. However, this method not only requires pre-scanning before measurement, but also cannot figure out the optimal approaching angle when adjacent profiles vary greatly. Dai also found that the probe with flared tip did not work well in torsional oscillation mode because the flexure spring constant of flared tip is much smaller than the torsion spring constant of cantilever. Therefore, other researchers have devoted more effort to exploring new probe technology<sup>[15-18]</sup>.

In order to overcome the limitations of measuring narrow and deep trenches and improve the measurement efficiency and accuracy, we develop a 3D-AFM prototype and the corresponding scanning

method. Multiple piezo stages are used to construct a high-speed and high-precision scanning platform whose range reaches  $100\ \mu\text{m} \times 115\ \mu\text{m} \times 25\ \mu\text{m}$ , and compact optical lever is designed to track probe movement. Moreover, commercial critical dimensional (CD) probe with rectangular cantilever is tailored for smaller contact force in measurement, and adaptive angle scanning method is employed for 3D imaging.

## 1 3D-AFM system configuration

The principle diagram of the 3D-AFM is illustrated in Fig.1(a), and Fig.1(b) shows the photo of the prototype. Among all of its parts, the objective that is responsible for observing the position of probe, and sample is located above probe and optical lever. Visible light reflected from probe and sample passes through the beam splitter into the objective, producing real image. In addition, there is laser beam passing through the beam splitter. The position of the reflected laser can indicate cantilever deformation. Reflected laser is converted to voltage signal by the quadrant-position detector (QPD) and the preamplifier, and then is transmitted to controller. The controller is a self-developed multifunctional digital control system with DSP and FPGA as processors. It is responsible for feedback controlling, outputting drive signals of all scanners, sampling various analog signals, etc.

The following is detailed description of the combined scanning and positioning system, the cantilever deformation detecting system and the improved probe with flared tip.

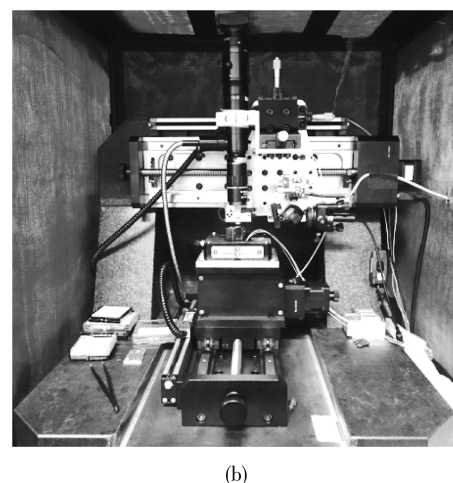
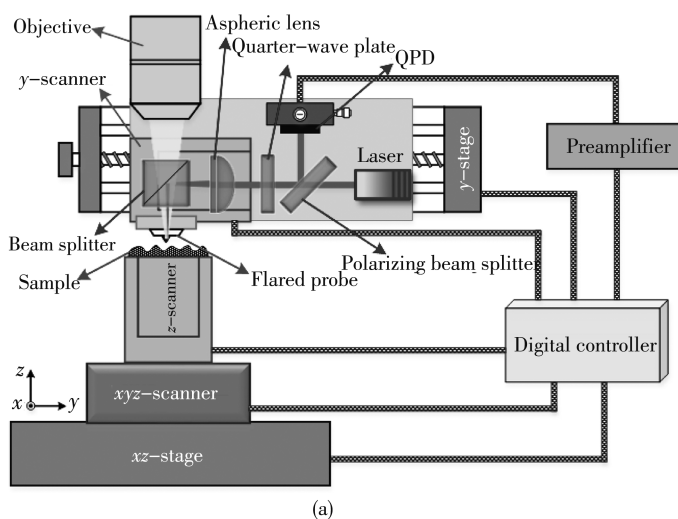


Fig. 1 Schematic diagram of 3D-AFM (a) and photo of prototype (b)

## 1.1 Combined scanning and positioning system

The combined scanning and positioning system includes a nano scanning platform and a large positioning platform. Considering that flared tip needs to approach surfaces along multiple directions for measuring 3D structure, the nano scanning platform should be capable of not only achieving rapid moving in at least two directions, but also ensuring as small displacement coupling error as possible. The nano scanning platform is composed of three piezo scanners produced by Physik Instrumente Ltd. The large positioning platform is composed of two motor positioning stages produced by Zolix Instruments Co., Ltd.

The overall structure is shown in Fig. 1(a). Sample stage is placed on  $z$ -scanner which is mainly used as  $z$ -axis feedback actuator. The  $z$ -scanner is mounted on  $xyz$ -scanner with  $100\ \mu\text{m} \times 100\ \mu\text{m} \times 10\ \mu\text{m}$  travel and 0.3 nm motion resolution.  $xyz$ -scanner is responsible for line scan. Probe-holder and some lenses are mounted on  $y$ -scanner which is used as  $y$ -axis feedback actuator.  $y$ -scanner and  $z$ -scanner have the same operational performance of 15  $\mu\text{m}$  travel and 0.05 nm resolution. Thus,  $y$ -scanner and  $z$ -scanner can take probe towards sample along an arbitrary direction precisely. To enlarge positioning range,  $y$ -scanner and  $xyz$ -scanner are assembled on two motor positioning stages,  $y$ -stage and  $xz$ -stage, respectively. Motor stages can achieve coarse positioning in a range of  $200\ \text{mm} \times 200\ \text{mm} \times 10\ \text{mm}$  with closed-loop resolution of below 1  $\mu\text{m}$ .

Although the movement direction of  $y$ -scanner is the same as  $y$ -axis of  $xyz$ -scanner and the movement direction of  $z$ -scanner is the same as  $z$ -axis of  $xyz$ -scanner, their performance requirements are different. Because  $xyz$ -scanner is for line scan,  $xyz$ -scanner has larger travel and lower moving speed. Whereas  $y$ -scanner and  $z$ -scanner are for feedback, they have higher moving speed and smaller travel. Besides, another situation must be considered that  $y$ -scanner and  $z$ -scanner are for both line scan and feedback when scanning area is smaller.

Because all of the scanners in the 3D-AFM are piezo nanopositioning stages, the bow effect generated by piezo tube can be essentially eliminated.

## 1.2 Cantilever deformation detecting system

In order to prevent the movement of  $y$ -scanner

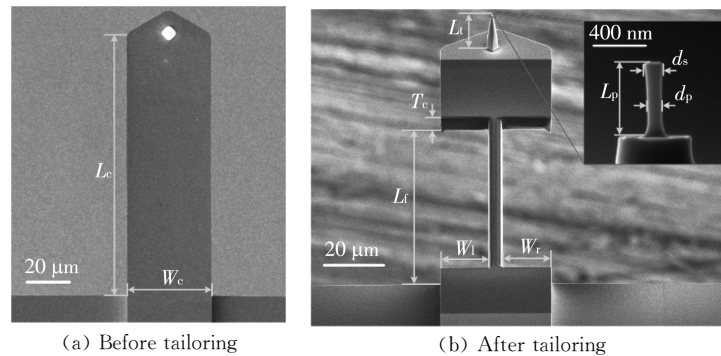
from affecting optical lever, we propose a traceable optical detector, and its working principle is as follows. As shown in Fig. 1(a), the collimated laser is split into two line polarized beams by the polarizing beam splitter. The transmitted line polarization is converted to circular polarization after it passing through a quarter-wave plate with its axis at  $45^\circ$  to the polarization axis of the incident beam. The circular polarization is then concentrated by aspheric lens, and half of the concentrated beam is reflected by the beam splitter to the cantilever. The optical length from the aspheric lens to the cantilever is just equal to the focal length. After that, the laser beam is reflected by the cantilever and then passes through the beam splitter and the aspheric lens again. The obtained parallel beam will be converted to line polarization whose polarization axis is perpendicular to the original line polarization axis so that it can reflect the polarizing beam splitter to the QPD. The output current signal from the QPD is converted to voltage signal via preamplifier and is finally transmitted to digital controller. When the cantilever deforms, the laser spot on the QPD will shift and the voltage will change.

During the assembly, we fixed the beam splitter, aspheric lens and probe-holder on  $y$ -scanner, accurately keeping the beam away from laser and the optical axis of aspheric lens concentric, which ensures that the spot irradiated on QPD does not shift and the spot on cantilever is not out of focus when  $y$ -scanner moves.

## 1.3 Improved probe with flared tip

Currently the only commercially probe available with flared tip is from CDR series product manufactured by Bruker Corporation. Fig. 2(a) shows the scanning electron microscope (SEM) image of the cantilever of CDR140 probe.

The highlight spot on the cantilever is the bottom view of flared tip. This probe is made of silicon. Because the spring constant of cantilever is much larger than that of flared tip, the tip is prone to bending while contacting with sidewall, causing measurement instability<sup>[19]</sup>. Hence, a method of improving probe by which the shape of cantilever is trimmed to reduce spring constants is proposed. The tailoring process is implemented using focused ion beam. The tailored probe is imaged by SEM, as shown in Fig. 2(b).


**Fig. 2 SEM images of CDR140 probe**

In Fig. 2,  $L_c$  is the distance from the center axis of flared tip to the fixed end of cantilever;  $W_c$  and  $T_c$  denote the width and the thickness of cantilever, respectively;  $L_t$  is the distance from the free end of tip to the cantilever base;  $l_p$  and  $d_p$  are the effective length and effective diameter of tip, respectively;  $d_s$  is the width of the protrusion on tip end;  $W_l$  and  $W_r$  are the cut width on the left and the right sides of cantilever while  $L_t$  is the cut length. Taking CDR140 probe as example, the its nominal values and tailored dimensions are shown in Table 1.

In order to investigate the mechanical properties of CDR140 probe, a geometric model is constructed and analyzed in finite element analysis software.

Table 2 shows the simulation results, where  $k_d$  represents the flexure spring constant of probe,  $k_p$  is the flexure spring constant of flared tip,  $k_t$  is the torsion spring constant of cantilever,  $k_e$  is the effective lateral spring constant of probe,  $a_d$  is the ratio of deflection angle to vertical displacement and  $a_e$  is the ratio of torsion angle to lateral displacement. After tailoring the cantilever,  $k_t$  decreases by nearly an order of magnitude, and  $a_e$  increases by nearly four times.

Therefore, the contact force applied on the tailored probe can be reduced in measurement, which is beneficial to measurement stability and probe lifetime.

**Table 1 Dimensions of CDR140 probe**

CDR140	$L_c$	$W_c$	$T_c$	$L_t$	$l_p$	$d_p$	$d_s$	$L_l$	$L_r$	$L_t$
Dimensions ( $\mu\text{m}$ )	115	35	3.3	15	0.45	0.08	0.14	80	15	15

**Table 2 Mechanical simulation results of CD140 probe**

	$k_d$ (N/m)	$k_t$ (N/m)	$k_p$ (N/m)	$k_e$ (N/m)	$a_d$ (rad/nm)	$a_e$ (rad/nm)
Before tailoring	35.0	768	11.3	10.0	$12.9 \times 10^{-6}$	$0.68 \times 10^{-6}$
After tailoring	5.1	96.5	11.3	5.2	$12.3 \times 10^{-6}$	$2.6 \times 10^{-6}$

## 2 Adaptive angle scanning method

In the measurement technology based on flared tip, how to adjust the approaching angle of tip and scanning direction to get an image featuring different slope surfaces is a critical problem<sup>[20]</sup>. Here, an adaptive angle scanning method is proposed. The scanning path on the line structure planned by this method is illustrated in Fig. 3, which well describes the basic principle of tracing surfaces.

In Fig. 3, the scanning path varies with slope angle. On top and bottom surfaces, the tip approaches at an angle of  $\theta_{t1}$ . When the contact force reaches the set value, the tip withdraws a distance of  $U_{tw}$  along the opposite direction. Certainly,  $U_{tw}$

should be long enough to rid the tip of adhesive force. The tip then moves a step length of  $S_{ty}$  along the positive  $y$ -axis to measure next area.

To prevent the tip from colliding with sidewall,  $\theta_{t1}$  should be slightly smaller than  $90^\circ$ . On left sidewall and right sidewall, measurement procedures are similar to that of top or bottom surface except the approaching angle and the scanning direction. On left sidewall, the approaching angle is set to be  $\theta_{t2}$  and the scanning direction is the positive  $z$ -axis with a step length of  $S_{tz}$ . On right sidewall, the approaching angle is set to be  $\theta_{t3}$  and the scanning direction is the negative  $z$ -axis with a step length of  $S_{tz}$ . To prevent the tip from flying away from the surface,  $\theta_{t2}$  should be larger than  $0^\circ$ . To prevent the tip from colliding with bottom surface,  $\theta_{t3}$  should be smaller than  $180^\circ$ .

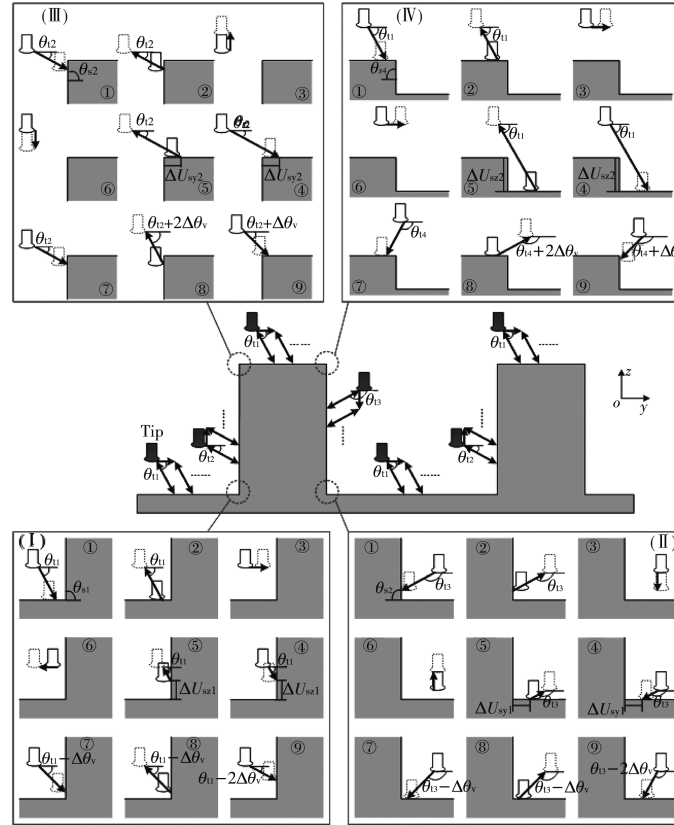


Fig. 3 Adaptive-angle scanning strategy on line structure. (I) shows how left-bottom corner is measured, (II) shows how right-bottom corner is measured, (III) shows how left-top corner is measured, and (IV) shows how right-top corner is measured

The remaining question is how to predict the slope angle. Here, it can be done by the coordinate values of adjacent points. Assuming that the tip is scanning on bottom surface and there is a sidewall with slope angle of  $\theta_{s1}$  in front of it, the height difference between two adjacent measurement points,  $\Delta U_{sy1}$ , can be approximately calculated by

$$\Delta U_{sy1} \approx \frac{S_{ty} \tan \theta_{s1} \tan \theta_{t1}}{\tan \theta_{s1} + \tan \theta_{t1}} \quad (1)$$

Hence, the slope can be roughly calculated from the height difference. When the tip is scanning on right sidewall with a slope angle of  $\theta_{s2}$ , the measured lateral roughness,  $\Delta U_{sy1}$ , can be expressed as

$$\Delta U_{sy1} \approx \frac{S_{tz}}{\tan(180^\circ - \theta_{i3}) - \tan(\theta_{s2})} \quad (2)$$

When the tip is scanning on left sidewall with a slope angle of  $\theta_{s3}$ , the measured lateral roughness,  $\Delta U_{sy2}$ , can be expressed as

$$\Delta U_{sy2} \approx \frac{S_{tz}}{\tan \theta_{s3} + \tan \theta_{t2}} \quad (3)$$

When the tip is scanning on top surface and there is a sidewall with slope angle of  $\theta_{s4}$ , which is smaller than  $0^\circ$ , in front of it, two situations need to be discussed separately. If  $\theta_{t1}$  is smaller than  $-\theta_{s4}$ , the height difference between two adjacent measurement

points,  $\Delta U_{sz2}$ , is equal to the height of top surface. If  $\theta_{t1}$  is larger than  $-\theta_{s4}$ ,  $\Delta U_{sz2}$  can be expressed as

$$\Delta U_{sz2} \approx \frac{S_{ty} \tan \theta_{t1} \tan \theta_{s4}}{\tan \theta_{t1} + \tan \theta_{s4}} \quad (4)$$

On four corners, the contours are measured by gradually changing the approaching angle while all scanning axes are disable. The insets of Fig. 3 show the details. For the measurement points of left-bottom corner, the approaching angle decreases from  $\theta_{t1}$  to  $\theta_{t2}$ . For left-top corner, the approaching angle increases from  $\theta_{t2}$  to  $\theta_{t1}$ . For right-top corner, the approaching angle increases from  $180 - \theta_{t1}$  to  $\theta_{t3}$ . For right-bottom corner, the approaching angle decreases from  $\theta_{t3}$  to  $\theta_{t1}$ .

If scanning path in Fig. 3 refers to trace scanning, retrace scanning path would be its mirror image. Through scanning once with the adaptive-angle scanning method, a complete 3D contour, including top surfaces, bottom surfaces, two opposite sidewalls and corners, can be obtained in relatively uniform pixel density.

### 3 Experimental results and analysis

A series of experiments are carried out to investigate the capability and performance of the

developed 3D-AFM.

First, we evaluate the measurement noise. After installing the tailored CDR140 probe on the 3D-AFM prototype, digital controller is ready to capture the voltage signal corresponding to cantilever deflection. In order to reduce the impact of thermal drift on noise evaluation, the sampling process is started for 3 h after the instrument is powered on. The sampling frequency is 100 kHz and the sampling time is 1 s. Fig. 4 shows sampling results. The peak-to-peak is about 8 mV and the standard deviation is 1.17 mV. The sensitivity can be obtained from the curve of voltage against vertical displacement, being about 70 mV/nm.

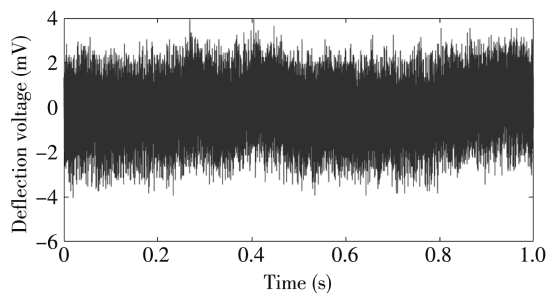


Fig. 4 Noise of voltage corresponding to cantilever deflection

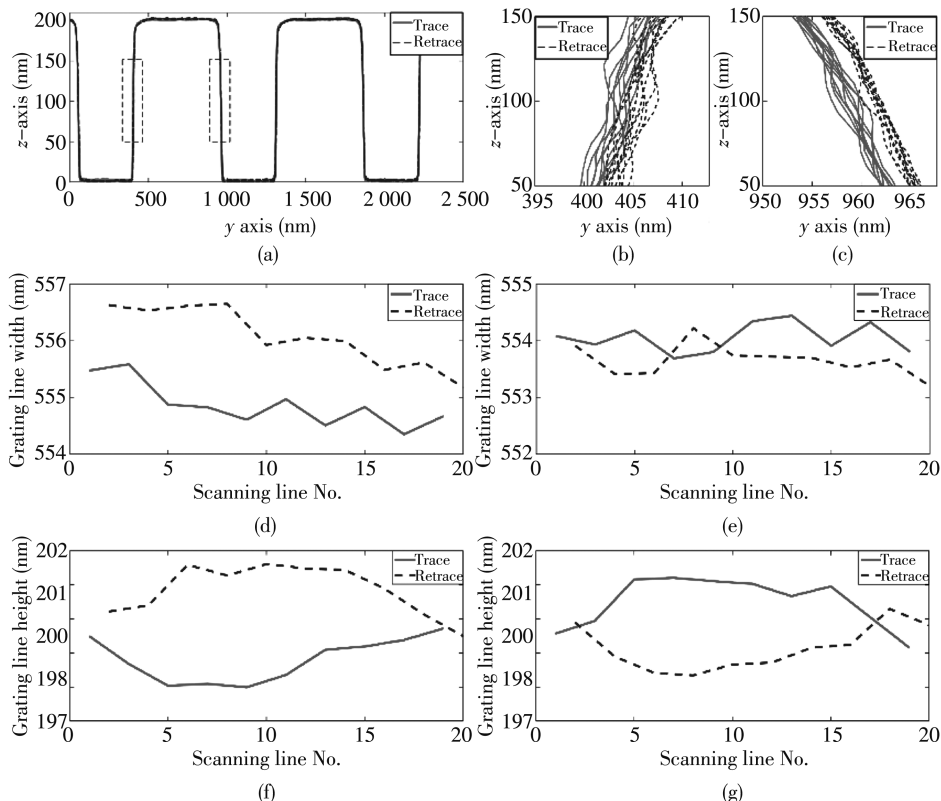


Fig. 5 Twenty measured profiles of grating standard on the same area: (a) zoomed-in view of left sidewall (b) and right sidewall (c), calculated line width of the first line structure (d) and the second line structure (e), and calculated line height of the first line structure (f) and the second line structure (g)

In order to evaluate the critical dimensions of grating, the data are further processed. Selecting the

As a result, the root-mean-square (RMS) value of vertical displacement noise is only 0.017 nm.

Next, a grating standard produced by LightSmyth Technologies, Inc. is measured by means of adaptive angle scanning method. The grating is made of silicon with a period of 833.3 nm, a line width of 416 nm and a line height of 200 nm. The probe is excited at near resonant frequency. The amplitude of cantilever is used to trigger the capture of displacement signal and the withdrawal behavior. The approaching angle is set as follows:  $\theta_{11} = 75^\circ$ ,  $\theta_{12} = 15^\circ$  and  $\theta_{13} = 165^\circ$ . The scanning step length is set as follows:  $S_{ty} = 8$  nm and  $S_{tz} = 8$  nm. With disabling  $x$ -axis scanning, 20 measurement profiles on the same area are obtained, as shown in Fig. 5, where ten of which are trace profiles and the others of which are retrace profiles. Every profile contains 500 data points. Apparently, all these profiles show a good agreement with each other. However, slight offset between the trace and the retrace can be seen if sidewalls are zoomed in. We suspect that this phenomenon is probably caused by the hysteresis of the piezoelectric actuator<sup>[21]</sup>.

middle 11 points on top surface for averaging and selecting the middle 11 points on bottom surface for

averaging, the difference of two mean heights is considered to be the grating height. The 11 points near half height of each sidewall are averaged, and the line or groove width can be derived from the difference of adjacent mean values. The calculated line width and line height are shown in Figs. 5(d)–(g). Although the offset between trace profiles and retrace profiles can also be reflected in the width and height, the measurement repeatability along the same scanning direction performs good, and the peak-to-peak value is better than 2.5 nm. Because the measurement image is the convolution of actual image and tip contour, the calculated line width is always larger than actual value. By subtracting the width of the protrusion on tip end from the measured value, we can get a more approximate line width that is about 416 nm.

Another experiment is taken on a pillar pattern. With respect to the pattern, a group of pillars with a diameter of about 240 nm and a height of about 150 nm are formed in hexagonal array on a silicon substrate. The distance between two adjacent pillars is about 600 nm. The pillar pattern is first measured in tapping mode using commercial AFM called as Dimension Icon, which is produced by Bruker Corporation. The applied probe is MESP. The

scanning range is  $2\ \mu\text{m} \times 2\ \mu\text{m}$ . The image pixels are set to be  $512 \times 256$ . Fig. 6(a) shows the measurement results. Then, the pillar pattern is measured by adaptive-angle scanning method using self-built 3D-AFM. The applied probe is tailored CDR140. The approaching angle is set as follows:  $\theta_{t1} = 80^\circ$ ,  $\theta_{t2} = 20^\circ$  and  $\theta_{t3} = 160^\circ$ . The scanning step length is set as follows:  $S_{ty} = 8\ \text{nm}$  and  $S_{tz} = 5\ \text{nm}$ . The image pixels are set to be  $400 \times 256$ . The obtained 3D image is shown in Fig. 6(b).

It can be seen from one zoomed-in profile that the pixel density of the image measured by Dimension Icon is dependent on the surface slope, with poor exhibition of the sidewall details. Moreover, the image from the commercial AFM is diluted seriously by conical tip, presenting a distorted sidewall contour. While in Fig. 6(b), the profile well characterizes the steep sidewalls. All corner shapes are formed through lots of measurement points. However, the pillar height calculated from two images has an offset of about 36 nm. The reason is that the two measurements are not the same area and the pillars on the pattern are not identical in shape. The pillars in Fig. 6(b) have pie-like stuffs depositing on the top. That is extremely like photoresist that is not removed during fabrication.

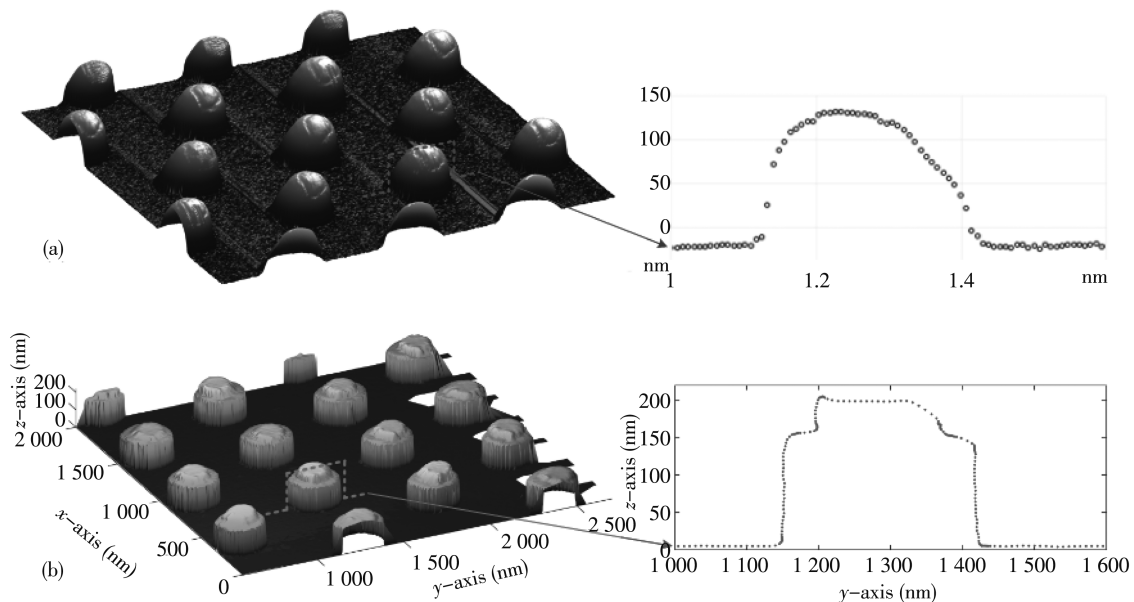


Fig. 6 Images of pillar pattern from Dimension Icon (a) and self-built 3D-AFM (b)

## 4 Conclusion

In this paper, a scheme of 3D-AFM based on tailored cantilever probe with flared tip and a scanning method is proposed. First, we introduce the overall structure of a 3D-AFM. By integrating two

high-speed linear scanners into AFM-head and sample stage respectively, fast displacement feedback on arbitrary direction without orthogonal coupling error is achieved. By designing a traceable optical path in which the laser beam can follow AFM-head movement, the spot position deviation is eliminated.

After tailoring the cantilever, the probe with flared tip represents smaller spring constant and the torsional sensitivity increases by near four times. The designed adaptive angle scanning method improves the measurement efficiency by changing approaching angle and scanning direction in real time. According to the noise test, the RMS value of the vertical displacement noise is less than 0.02 nm when the tip does not contact with sample. By measuring grating standard with slow scan axis being disable, both the line width and the line height presented a repeatability less than 2.5 nm. The high-quality 3D image of a pillar pattern further validates the measurement reliability of the 3D-AFM and the method, in which all surfaces, including top surface, bottom surface, two opposite sidewalls and four corners, are characterized clearly.

## References

- [1] Morimoto T, Kuroda H, Minomoto Y, et al. Atomic force microscopy for high aspect ratio structure metrology. *Japanese Journal of Applied Physics*, 2002, 41(6S): 4238.
- [2] Murayama K, Gonda S, Koyanagi H, et al. Three-dimensional metrology with side-wall measurement using tilt-scanning operation in digital probing AFM. In: *Proceedings of Metrology, Inspection, and Process Control for Microlithography XX*. International Society for Optical Engineering, 2006: 615216.
- [3] Hussain D, Ahmad K, Song J, et al. Advances in the atomic force microscopy for critical dimension metrology. In: *Proceedings of Measurement Science and Technology*, 2016, 28(1): 012001.
- [4] Mancevski V, McClure P F. Development of a dual-probe Caliper CD-AFM for near model-independent nanometrology. *Metrology, Inspection, and Process Control for Microlithography XVI*. International Society for Optical Engineering, 2002: 83-91.
- [5] Foucher J, Thérèse R, Lee Y, et al. Introduction of next-generation 3D AFM for advanced process control. In: *Proceedings of SPIE Advanced Lithography*, International Society for Optics Engineering, 2013: 868106.
- [6] Foucher J, Filippov P, Penzkofer C, et al. Manufacturing and advanced characterization of sub-25nm diameter CD-AFM probes with sub-10nm tip edges radius. In: *Proceedings of SPIE Advanced Lithography*. International Society for Optical Engineering, 2013: 868111-868116.
- [7] Dixson R, Ng B P, Orji N. Effects of lateral tip control in CD-AFM width metrology. *Measurement Science and Technology*, 2014, 25(9): 094003.
- [8] Murayama K, Gonda S, Koyanagi H, et al. Side-wall measurement using tilt-scanning method in atomic force microscope. *Japanese Journal of Applied Physics*, 2006, 45(6S): 5423-5428.
- [9] Cho S J, Ahn B W, Kim J, et al. Three-dimensional imaging of undercut and sidewall structures by atomic force microscopy. *Review of Scientific Instruments*, 2011, 82(2): 023707.
- [10] Xie H, Hussain D, Yang F, et al. Atomic force microscope caliper for critical dimension measurements of micro and nanostructures through sidewall scanning. *Ultramicroscopy*, 2015, 158: 8-16.
- [11] Xie H, Hussain D, Yang F, et al. Development of three-dimensional atomic force microscope for sidewall structures imaging with controllable scanning density. *IEEE/ASME Transactions on Mechatronics*, 2016, 21(1): 316-328.
- [12] Martin Y, Wickramasinghe H K. Method for imaging sidewalls by atomic force microscopy. *Applied Physics Letters*, 1994, 64(19): 2498-2500.
- [13] Dai G, Hässler-Grohne W, Hüser D, et al. New developments at PTB in 3D-AFM with tapping and torsion AFM mode and vector approach probing strategy. In: *Proceedings of SPIE Defense, Security, and Sensing*, International Society for Optical Engineering, 2011: 80360V.
- [14] Dai G, Hässler-Grohne W, Hüser D, et al. Development of a 3D-AFM for true 3D measurements of nanostructures. *Measurement Science and Technology*, 2011, 22(9): 094009.
- [15] Liu H, Klonowski M, Kneeburg D, et al. Advanced atomic force microscopy probes: Wear resistant designs. *Journal of Vacuum Science & Technology B: Microelectronics and Nanometer Structures Processing, Measurement, and Phenomena*, 2005, 23(6): 3090-3093.
- [16] Foucher J, Faurie P, Dourthe L, et al. Hybrid Metrology & 3D-AFM Enhancement for CD Metrology Dedicated to 28 nm Node and Below Requirements. In: *Proceedings of AIP Conference American Institute of Physics*, 2011: 763802.
- [17] Foucher J, Schmidt S W, Penzkofer C, et al. Overcoming silicon limitations; new 3D-AFM carbon tips with constantly high-resolution for sub-28nm node semiconductor requirements. In: *Proceedings of Metrology, Inspection, and Process Control for Microlithography XX-VI*, International Society for Optical Engineering, 2012: 832432.
- [18] Ageev O A, Bykov A V, Kolomiitsev A S, et al. Study of modification methods of probes for critical-dimension atomic-force microscopy by the deposition of carbon nanotubes. *Semiconductors*, 2015, 49(13): 1743-1748.
- [19] Zhang R, Wu S, Liu L, et al. A CD probe with a tailored cantilever for 3D-AFM measurement. *Measurement Science and Technology*, 2018, 29(12): 125011.
- [20] Zhang R, Wu S, Liu L, et al. Adaptive-angle-scanning method for three-dimensional measurement with AFM. *Measurement Science and Technology*, 2019, 30(9): 095005.
- [21] Liu Y, Shan J, Gabbert U, et al. Hysteresis and creep

modeling and compensation for a piezoelectric actuator using a fractional-order Maxwell resistive capacitor ap-

proach. *Smart Materials and Structures*, 2013, 22(11): 115020.

## 一种基于改进型裙摆探针的三维原子力显微技术

张 锐<sup>1,2</sup>, 吴 森<sup>1,2</sup>, 肖莎莎<sup>1,2</sup>, 胡晓东<sup>1,2</sup>, 施玉书<sup>3</sup>, 傅 星<sup>1,2</sup>

(1. 天津大学 精密测试技术及仪器国家重点实验室, 天津 300072;

2. 天津大学 南昌微技术研究院, 天津 300072;

3. 中国计量科学研究院, 北京 100029)

**摘 要:** 针对微纳米结构的真三维形貌无损检测需求, 研制了基于裙摆型针尖(Flared tip)的三维原子力显微镜(3D-AFM)。设计了一种高精度扫描平台结构, 通过同时移动探针和样品实现快速伺服反馈, 并利用组合式纳米定位台来保证位移的线性度和正交性。为了消除因 AFM 测头移动引起的信号偏差, 设计了随动式光杠杆系统用于检测悬臂梁的形变量。此外, 提出了一种基于商用裙摆探针的悬臂梁裁剪方法, 可减小测量过程中针尖横向受力。将改进型探针安装到 3D-AFM 系统上, 利用自适应矢量逼近扫描策略进行了多种样品的 3D 测量实验。实验结果表明, 样机的垂直方向位移噪声(RMS)优于 0.1 nm, 高/宽测量重复性(峰峰值)优于 2.5 nm。

**关键词:** 三维原子力显微镜; 裙摆型针尖; 扫描器; 光杠杆; 矢量扫描

**引用格式:** ZHANG Rui, WU Sen, XIAO Sha-sha, et al. Three-dimensional atomic force microscopy based on tailored cantilever probe with flared tip. *Journal of Measurement Science and Instrumentation*, 2020, 11(4): 388-396. [doi: 10.3969/j.issn.1674-8042.2020.04.011]